Nucleic Acids Research, 2024, **52**, 1258–1271
https://doi.org/10.1093/nar/gkad1151
Advance access publication date: 4 December 2023
Molecular Biology

Alternative cleavage and polyadenylation of the Ccnb1 mRNA defines accumulation of cyclin protein during the meiotic cell cycle

Xiaotian Wang [1,2,3], Fang-Shiuan Leung[2,4,5,6], Jeffrey O. Bush[2,4,5,6] and Marco Conti[1,2,3,*]

[1]Center for Reproductive Sciences, University of California, San Francisco, CA 94143, USA
[2]USA Eli and Edythe Broad Center of Regeneration Medicine and Stem Cell Research, University of California, San Francisco, CA 94143, USA
[3]Department of Obstetrics, Gynecology and Reproductive Sciences, University of California, San Francisco, CA 94143, USA
[4]Department of Cell and Tissue Biology, University of California San Francisco, San Francisco, CA 94143, USA
[5]Program in Craniofacial Biology, University of California San Francisco, San Francisco, CA 94143, USA
[6]Institute for Human Genetics, University of California San Francisco, San Francisco, CA 94143, USA

*To whom correspondence should be addressed. Tel: +1 415 476 2695; Fax: +1 415 502 7866; Email: Marco.Conti@ucsf.edu

Abstract

Progression through the mitotic and meiotic cell cycle is driven by fluctuations in the levels of cyclins, the regulatory subunits controlling the localization and activity of CDK1 kinases. Cyclin levels are regulated through a precise balance of synthesis and degradation. Here we demonstrate that the synthesis of Cyclin B1 during the oocyte meiotic cell cycle is defined by the selective translation of mRNA variants generated through alternative cleavage and polyadenylation (APA). Using gene editing in mice, we introduced mutations into the proximal and distal polyadenylation elements of the 3′ untranslated region (UTR) of the *Ccnb1* mRNA. Through *in vivo* loss-of-function experiments, we demonstrate that the translation of mRNA with a short 3′ UTR specifies Cyclin B1 protein levels that set the timing of meiotic re-entry. In contrast, translation directed by a long 3′ UTR is necessary to direct Cyclin B1 protein accumulation during the MI/MII transition. These findings establish that the progression through the cell cycle is dependent on the selective translation of multiple mRNA variants generated by APA.

Graphical abstract

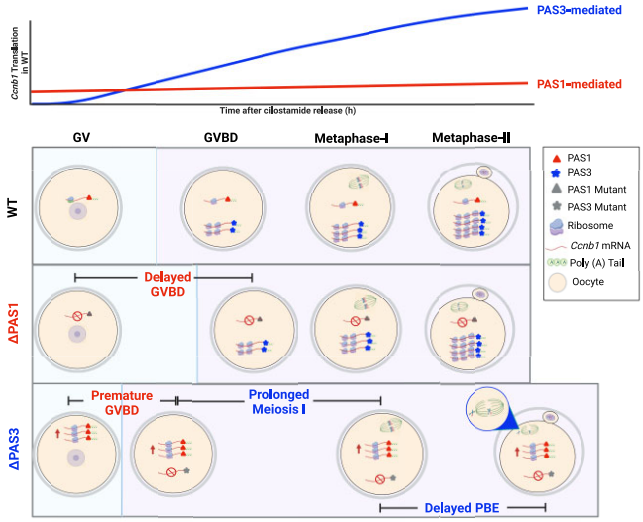

Introduction

Together with the regulation of transcription, a rich repertoire of post-transcriptional modifications fine-tunes gene expression in a cell. Alternate cleavage and polyadenylation (APA) is one of these post-transcriptional mechanisms that add layers of control to protein synthesis. In addition to 5′ end modifications of an mRNA and upstream region APA, 3′ UTR-APA is a widespread mechanism that generates distinct 3′ ends in Pol II-synthesized transcripts (1). In this process, *cis-acting* polyadenylation signals (PAS) recruit large protein complexes that direct alternative cleavage and polyadenylation of an mRNA (1,2). The heterogeneity in the 3′ UTRs

Received: June 16, 2023. **Revised:** November 1, 2023. **Editorial Decision:** November 13, 2023. **Accepted:** November 14, 2023

generated by this mechanism, in turn, defines the turnover and/or rate of translation of the mRNA isoforms and often provides information for targeting mRNA synthesis to specific subcellular compartments (1,3). Numerous examples of APA have established the tissue specificity of these events as well as their involvement in cell proliferation and differentiation (1,3–5). One of the best-studied consequence of APA is the generation of mRNA isoforms that are either resistant or subject to microRNA-mediated repression or destabilization (6,7). APA is regulated during organ development, as transcripts with long 3′ UTRs generated by APA are preferentially expressed in the brain (8–11). Similarly, T lymphocyte proliferation induced by blocking CD3/CD28 function causes a shift in the expression of mRNAs with short 3′ UTRs (12). Moreover, widespread preferential use of proximal versus distal PAS domains is associated with oncogenic transformation (13,14). Here, we will explore the function of novel variants of cyclin mRNAs generated by APA during the unique meiotic cell cycle.

Gamete development is essential to generate oocytes and spermatozoa competent to support fertilization and the generation of a totipotent zygote (15–17). After a period of prolonged growth supported by active transcription, fully grown oocytes enter a quiescent G2-like state (dictyate) in preparation for the final meiotic divisions (16). These divisions are essential to generate a haploid gamete competent for fertilization and embryo development (18). Oocyte maturation involves a first asymmetrical meiotic division (MI) with extrusion of the first polar body (PB1), followed by entry into the second division and arrest at the metaphase II (MII) stage (19). The properties and timing of progression through these transitions are dependent on cycles of activation and inactivation of the maturation-promoting factor (MPF) complex composed of the CDK1 kinase in association with its cyclin regulatory subunits (20,21). Although MPF functions as the master regulator of both mitosis and meiosis, the unique dynamics of the meiotic cell cycle are the result of a myriad of regulatory loops for the fine-tuning, timing, and activity of the core mitotic cell cycle components.

The transition between a steady-state where a CDK1/cyclin complex is inactive (pre-MPF) and the rapid switch-like reentry into prophase induced by activation of MPF relies on multiple events that set the cyclin protein steady-state levels and the phosphorylation status of the components of the MPF complex. Mammalian oocytes express three M-phase cyclins: Cyclin B1, B2 and B3 (22,23). Although early reports concluded that Cyclin B1 was the cyclin involved in CDK1 regulation during meiosis (24), more recent studies have revealed a role also for Cyclin B2 and B3 during this transition. Whereas Cyclin B3 may play a role later during metaphase (25–27), the steady-state levels of both Cyclin B1 and B2 set the pre-MPF levels required for a rapid switch-like transition to prophase and dissolution of the nuclear membrane, which is also known as germinal vesicle breakdown (GVBD) (25,26,28,29). Cyclin B1 and B2 proteins undergo continuous turnover in the quiescent GV state as demonstrated by the finding that inhibition of the APC/C complex by small molecule inhibitors or by loss-of-function of the APC regulator Fzr1/Cdh1 causes unstable GV state and/or premature meiotic re-entry (28,30–32). At the same time as regulated degradation, the synthesis of cyclins in GV depends on the tightly regulated translation of the mRNAs that encode these cyclins (33). *Ccnb2* mRNA is translated at a rate that is 3–5-fold higher than *Ccnb1* in quiescent GV-stage oocytes, and loss-of-function studies have documented that this cyclin plays a role in setting the timing and the properties of the cell cycle re-entry in mouse oocytes (29).

It is well established that the RNA binding protein CPEB1 (cytoplasmic polyadenylation element binding protein 1) is essential for the regulation of cyclin mRNA translation in both frog and mouse oocytes (34). Moreover, PAS elements play a significant role in the interaction of this RBP (RNA binding protein) with an mRNA (35). Several *cis-acting* elements interacting with CPEB1 have been mapped in both Xenopus and mouse *Ccnb1* 3′ UTR (35–37). Binding to this RBP is required for the repression of translation in quiescent GV oocytes and for polyadenylation and increased translation after meiotic cell cycle re-entry (35). In frog oocytes, the location and number of CPEs present in the cyclins constitute a combinatorial code that defines the timing of cyclin mRNAs (38). Mutagenesis of the CPE elements results in de-repression in GV-arrested mouse oocytes and prevents the translational activation during meiotic re-entry (35,36). Activation of translation is reduced in oocytes lacking CPEB1 (37). The molecular mechanism proposed is that CPEB1 interacts with the CPSF (Cleavage and polyadenylation specificity factor) protein complex and recruits it to PAS element. Specifically, phosphorylation by one or more kinases increases the affinity of CPEB1 for CPSF and stabilizes the CPSF interaction with this element, as determined by co-immunoprecipitation (39,40). Mutagenesis of PAS elements in the *Ccnb1* mRNA greatly reduces translation (35).The interaction with CPSF promotes the expulsion of the deadenylase PARN (Poly(A) ribonuclease) from the complex and recruitment of components required for polyadenylation or for protection of the poly(A) tail (PABP, Poly(A)-binding protein). However, the presence of PARN in the repressive complex has been challenged by biochemical and mass spectrometry studies (41,42).

In spite of the overall repression of translation of the *Ccnb1* mRNA in quiescent oocytes, however, steady-state levels of Cyclin B1 may have a function at this stage. In a previous study, we proposed that *Ccnb1* mRNAs expressed in the oocytes are heterogeneous because of the presence of 3′ UTRs of different lengths, with the mRNA with the short 3′ UTR translated at a rate estimated to be 10 times higher than that of the mRNAs with the longer 3′ UTRs in quiescent GV oocytes (36). This heterogeneity is likely caused by APA of the nascent *Ccnb1* transcript. Here, we have investigated the functional consequences of generation of heterogenous mRNA isoforms and the distinct roles of these isoforms in Cyclin B1 translation regulation during the meiotic cell cycle *in vivo*. We provide evidence that Cyclin B1 mRNAs with short and long 3′ UTRs define the pattern of synthesis and the levels of Cyclin B1 protein throughout the meiotic cell cycle.

Materials and Methods

Animals

Mice were housed at a constant temperature (18–23°C) and a controlled light cycle (12 h light/dark), with food and water provided ad libitum. Animal-use protocols were approved by the Institutional Animal Care and Use Committee (IACUC) of the University of California at San Francisco (AN197697-00), and all experiments were conducted in accordance with the specified guidelines.

Gene editing of the 3′ UTR of the Ccnb1 locus

Mutant mice were generated by CRISPR/Cas9 gene editing and homologous directed repair (HDR) as follows. crRNA targets for PAS1 and PAS3 were designed (PAS1 crRNA: 5′-GUU UAC UUG CUC UUC AAU AA-3′; PAS3 crRNA: 5′-UCA AGU UGA AUA AAA UUU AU-3′), together with exogenous DNA templates (single-stranded oligodeoxynucleotides (ssODN)) to ensure precise incorporation of the desired mutation via HDR for each of the targeted PAS element (PAS1 ssODN: 5′-GCC TGT ACA TAG GAT ACC TAC CGT GTT TAC TTG CTC TTC AGG AAG AAT TCT GAC TTC TCA TTT TAC ATA GCT TAA CTC ATT TGA ATG TTG-3′; PAS3 ssODN: 5′-CAT TTG CTG TTT TAA TTT ATA CAT CTG ATA TCA AGT TGA GGA AAA TTG AAT TCT GGA AAG CTT TCA CAA TTC TCA TTT GCC CTT TTG ACT G-3′), and synthesized by IDT (www.idtdna.com). To deliver them, we performed the iGONAD (improved-Genome editing via Oviductal Nucleic Acids Delivery) procedure according to published protocols (43,44). Briefly, 30 μM crRNA/tracrRNA and 1mg/ml Cas9 protein were pre-incubated to form an RNP complex and combined with 1mg/ml ssODN for direct injection into the oviducts of 0.7-day pregnant CD1 females followed by *in vivo* electroporation for embryo delivery. For genotyping, tail biopsies were collected and either lysed for DNA extraction and EcoRI digestion after PCR or used for Sanger sequencing (Supplementary Figure 1). At least two founders per mouse line were generated, and progenies were maintained in a CD1 and C57BL/6J mixed background and used after F3/F4 backcrossing.

Oocyte collection and microinjection

Female mice (21–23-days old) were primed with 5 I.U. of pregnant mare gonadotropin (PMSG, MyBioSource, MBS173236) and sacrificed 44–48 h later to collect GV-arrested oocytes. Cumulus-oocyte complexes (COCs) were retrieved from antral follicles and mechanically denuded in HEPES modified Minimum Essential Medium Eagle (Sigma-Aldrich, M2645) supplemented with 1μM cilostamide (Calbiochem, 231085). Oocyte *in vitro* maturation was performed at 37°C with 5% CO_2 in Minimum Essential Media (MEM)-α (Gibco, 12561–056) supplemented with 0.23mM sodium pyruvate and penicillin–streptomycin. For microinjection, denuded GV-arrested oocytes were injected with 5–10 pl of 12.5 ng/μl mRNA construct using a FemtoJet Express programmable microinjector with an Automated Leica microinjection Microscope System (LEICA DMI 4000 B). After pre-incubation, oocytes were then released from cilostamide and matured *in vitro* at 37°C with 5% CO_2 under time-lapse microscopy equipped with a Nikon Eclipse T2000-E.

Time-lapse microscopy and reporter assay

Time-lapse microscopy was performed under a Nikon Eclipse T2000-E equipped with a mobile stage and an environmental chamber at 37°C and 5% CO_2. For the experiments involving reporter assays, plasmids were generated by fusing the Ypet ORF to the different *Ccnb1* 3′ UTRs. For the rescue experiments, the mouse *Ccnb1* ORF was fused to either the PAS1 short or the PAS3 long 3′UTR. Linearized cDNAs were *in vitro* transcribed using the mMESSAGE mMACHINE T7 Transcription Kit (AM1344, Invitrogen). The *in vitro* transcribed mRNA coding for the reporters was microinjected along with polyadenylated mRNA coding for mCherry. The ratios of Ypet fluorescence and the maximum level of mCherry signal were used to plot the translation accumulation during time-lapse. Translation rates were calculated using Ypet/mCherry ratios as the slope obtained from simple linear regression curves from the linear portion of the time course. In the rescue experiments, oocytes were microinjected with *Ccnb1* ORF fused to either PAS1 short or PAS3 long 3′UTR, and then recorded for *in vitro* maturation under time-lapse microscopy. Oocytes acting as controls were injected with the vehicle only.

Immunofluorescence analysis

The oocytes were fixed with 4% paraformaldehyde in DPBS with 0.05% Triton-X for 30 min at 37°C, then washed and blocked in DPBS supplemented with 5% serum, 1% antibiotic/antimycotic solution, and 0.05% Triton-X. Specific primary antibody was used to detect acetylated α-tubulin (T6793, Sigma Aldrich, 1/500 dilution). In brief, fixed oocytes were incubated with primary antibody overnight at 4°C, then washed several times and transferred to specific Alexa Fluor conjugated 488 secondary antibody (A-11017, ThermoFisher) for 1h incubation at 37°C. DNA was counterstained with 6μl Vectashield mounting media containing DAPI (H-1200, Vector Laboratories). Images were acquired on a Zeiss LSM980 confocal microscope.

Western blotting

Oocytes were collected in 0.1% PVP in DPBS and then transferred to a tube with 1X Laemmli buffer (1610747, Bio-Rad) supplemented with β-mercaptoethanol, protease and phosphatase inhibitors (87 786, 78 420, ThermoFisher) and heated at 95°C for 5 min. In preparation for analysis, oocyte lysates were re-boiled at 95°C for 5 min, then separated on 8% polyacrylamide gels and transferred to polyvinylidene difluoride (PVDF) membranes. Following transfer, the membranes were blocked in Tris-buffered saline supplemented with 0.05% Tween 20 (TBST) containing 5% nonfat milk powder for 1 h at room temperature, then incubated at 4°C overnight with specific primary antibodies (1:1000 dilution) for the detection of the following proteins: Cyclin B1 (4138, Cell Signaling), Cyclin B2 (AF6004, R&D Systems), p-ERK1/2 (05–797R, EMD Millipore), and DDB1 (ab109027, Abcam). The following day, the membranes were washed in 1× TBST several times and then incubated with HPR-conjugated secondary antibodies (anti-Rabbit: NA934VS, Cytiva; anti-goat: HAF017, ThermoFisher) for 2 h at room temperature. ECL (170–5061, Bio-Rad) was used for chemiluminescent detection, and ImageJ was used for quantification.

In vitro CDK1 kinase assay

Oocytes were collected in 5 μl of 0.1% PVP in DPBS and mixed with 30 μl of 2× kinase buffer (100 mM Hepes, 30 mM $MgCl_2$, 2 mM EGTA, 10 mM $CaCl_2$, 2 mM DTT, 2 μg/ml leupeptin, 2 μg/ml aprotinin, 2 μM okadaic acid). Oocytes were lysed by freeze-and-thawing three times using liquid nitrogen. After adding 0.1 mM ATP, 10 mM DTT, and 2 μg of recombinant peptide GST-PP1 as the substrate, the lysates were incubated at 35°C in a water bath for 15 min. Reaction was immediately stopped by boiling at 95°C within Laemmli buffer supplemented with β-mercaptoethanol for 5 min. CDK1 activity was quantified by measuring the phosphorylated T320 of the total PP1-GST substrate using western blot analysis.

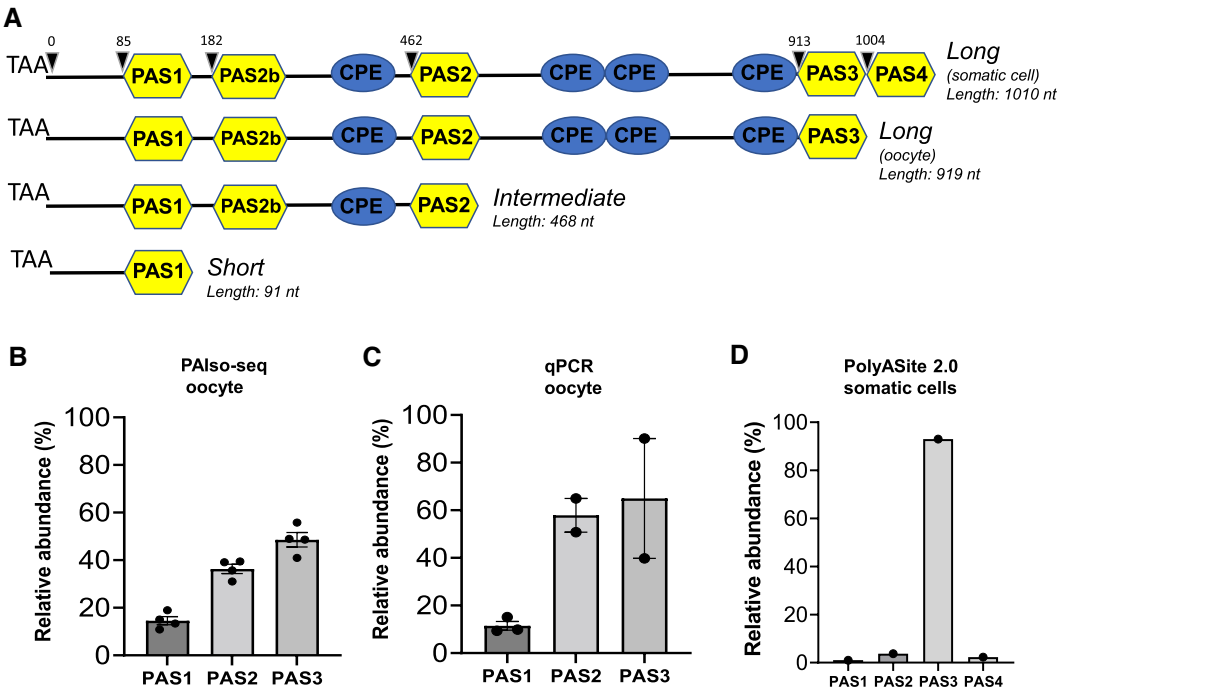

Figure 1. Differential usage of PAS elements in the *Ccnb1* 3′ UTR in oocyte versus somatic cells. (**A**) Representative scheme depicting the long, intermediate, and short 3′ UTRs of *Ccnb1* mRNA in both oocytes and somatic cells. PAS elements are highlighted in yellow, and regulatory CPE *cis*-acting elements are shown in blue. (**B**) Relative abundance of *Ccnb1* 3′ UTRs generated by different PAS element usage in mouse oocytes. Data were mined from the PAIso-seq dataset (45,46). Reported is the mean ± SE of four independent determinations. (**C**) PCR data using primers that detect the boundary between the sequence and the polyadenylation for each PAS-dependent 3′ UTR in mouse oocytes. Average and range of two biological independent determinations. (**D**) PolyASite 2.0 APA atlas data for PAS utilization in mouse somatic cells.

Statistical analysis

All data are presented as the Mean ± SEM from a minimum of three independent experimental replicates using distinct biological samples. GraphPad Prism 9 was used for data analysis and preparation of the graphs. The data were analyzed by either two-tailed, unpaired, or paired *t*-test, or by non-parametric Mann–Whitney test for comparison of two groups. Differences were considered to be significant when $P \leq 0.05$. Analysis of the time lapse microscopy data using Klomogorov–Smirnov test confirmed the significance of the differences calculated with the Mann–Whitney test. ImageJ and Metamorph were used for data collection and quantification from Western blot and reporter assay, respectively.

Results

Mouse *Ccnb1* mRNAs contain multiple 3′ UTR PAS elements, and oocytes use a unique alternative polyadenylation pattern

In our previous study (36), we reported the presence of three PAS elements (PAS1, PAS2 and PAS3) in the 3′ UTR of the mouse *Ccnb1* mRNA. Upon re-evaluation of the 3′ UTR sequence of this mRNA, we have identified two additional potential PAS elements. For consistency with our previous report, we have designated these two putative elements as PAS2b and PAS4 (Figure 1A). In order to assess the cell utilization of these two additional elements as well as that of the previously identified elements in mouse oocyte, we used two complementary methods. These include mining of a deposited PAIso-seq dataset, a collection of poly(A) boundaries used in GV oocytes (45,46), as well as quantitative PCR using primers that detect the boundary between the UTR sequence and the polyadenylation. Both methods gave comparable results detecting boundaries with a percentage usage of 11–15% for PAS1, 35–50% for PAS2 and 50–64% for PAS3 (Figure 1B,C). Usage of PAS2b and PAS4 could not be detected by mining the PAIso-seq datasets. The absence of sequence around the PAS4 in mRNA from mouse oocytes was further confirmed by PCR (Supplementary Figure 2A) and by mapping of the RNA-seq read distribution in the 3′ UTR of *Ccnb1* using our published datasets (37) (Supplementary Figure 2B). Based on these observations, we conclude that *Ccnb1* mRNA is expressed in oocytes with three 3′UTR-APA variants, one yielding a very short 3′ UTR of 91 nucleotides, and two with longer 3′ UTRs of 468 nt for PAS2 and 919 nt for PAS3.

PAS utilization in mouse somatic cells was determined by analyzing the PolyASite 2.0 APA atlas (https://polyasite.unibas.ch/) (47). In somatic cells, PAS3 is used with the highest frequency, followed by PAS2 and PAS4, while PAS1 was utilized at 1% frequency (Figure 1D and Supplementary Table 1). Hence, there is a notable divergence in alternative polyadenylation usage between mouse female gametes and somatic cells. It is worth noting that the sequence surrounding PAS1 is conserved across all investigated species (Supplementary Figure 3). For the subsequent studies, our analyses focused on the PAS elements employed in mouse oocytes.

Disruption of PAS elements in the mouse *Ccnb1* locus by gene editing

To explore the *in vivo* function of the PAS elements present within the *Ccnb1* 3′ UTR, we used CRISPR/Cas9 gene-editing

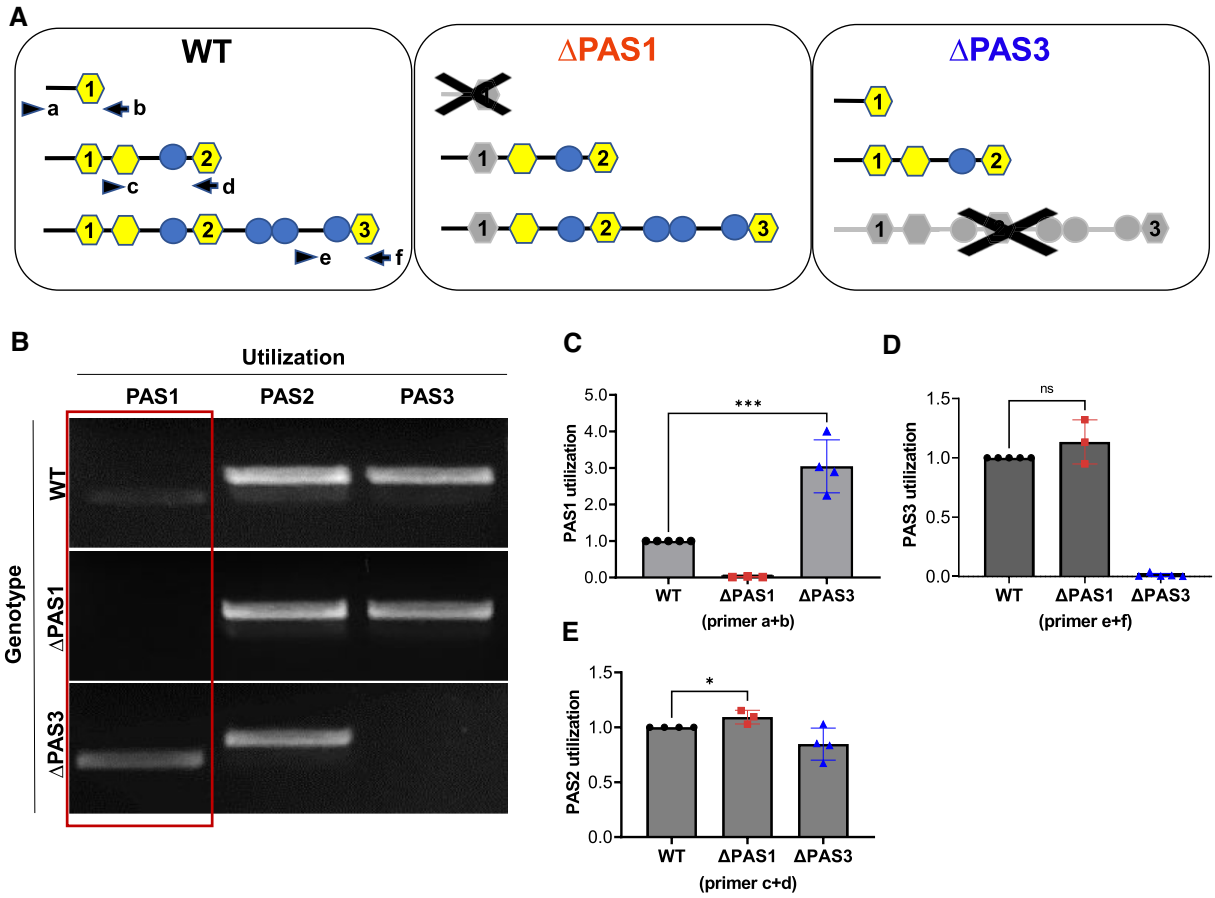

Figure 2. Disruption of PAS elements (PAS1 and PAS3) in the mouse *Ccnb1* locus by CRISPR Cas9 gene-editing. (**A**) Representative schemes showing the WT *Ccnb1* mRNA 3′ UTR, the *Ccnb1* 3′ UTR with PAS1 mutation, and the *Ccnb1* 3′ UTR with PAS3 mutation. PAS elements are highlighted in yellow, and CPE elements are shown in blue. (**B**) Representative ethidium bromide gel images of PCR products depicting the utilizations of PAS1, PAS2 and PAS3 respectively in WT and the mutant oocytes. Densitometric quantifications of the utilizations of PAS1 (**C**), PAS2 (**E**) and PAS3 (**D**) from WT and the mutant oocytes. Experiments were repeated at least three times. Statistical significance was assessed using unpaired *t*-test (*$P \leq 0.05$, ***$P \leq 0.001$, ns, not significant).

to perform homology-directed repair to generate two mouse lines (Figure 2A). In one mouse line, we introduced a mutation in exon 9 of the *Ccnb1* locus on chromosome 13 to disrupt the proximal PAS1 (AATAAA to AGGAAA) (ΔPAS1) and generate an EcoRI restriction fragment length polymorphism (RFLP) for genotyping purposes (Supplementary Figure 4A). In the other mouse line, the distal PAS used in the oocytes was mutated (ΔPAS3) following a similar strategy (Supplementary Figure 4B). Given that several *Ccnb1* pseudogenes are present in the mouse genome, the successful homologous recombination in the *Ccnb1* locus in chromosome 13 was verified by sequencing of tail genomic DNA and by EcoRI restriction digestion of the amplified genomic sequences. Chromosome 13 *Ccnb1* DNA sequence can be distinguished from pseudogene sequences by the presence of introns and by several diagnostic SNPs (Supplementary Figure 4A,B). Of note, when mRNA was extracted from mouse oocytes, reverse transcribed and sequenced, we were unable to detect any mRNA corresponding to these pseudogenes. The transmission of the mutated allele followed the Mendelian ratio. Mating of heterozygous mice yielded homozygous mice for either the PAS1 or PAS3 mutants with no overt phenotype (Supplementary Figure 5).

RNAs from oocytes from both WT and mutant females were extracted and reverse transcribed to cDNAs using two pairs of primers targeting the polyadenylation boundaries of each PAS plus a 15-base A-tail (Supplementary Table 2) to detect mRNA/ poly(A) boundaries in mouse oocytes. Signals were quantified by the intensities of ethidium bromide gel bands after PCR amplification. A weak signal was observed when using PAS1-specific primers in WT mice, whereas predominant PAS2 and PAS3 bands were detected (Figure 2B). In mutant oocytes, no signals were detected for PAS1 or PAS3 in their respective mutant oocytes, confirming the disruption of the PAS elements (Figure 2B–D). Surprisingly, an approximately 2–3-fold increase of PAS1 utilization was observed in PAS3 mutant mouse oocytes (Figure 2B, C). We also observed a slight increase in PAS2 usage upon disruption of PAS1 (Figure 2B,E). Moreover, the two mutations introduced did not have a major effect on the overall *Ccnb1* transcript levels, as total mRNA levels were either not affected or slightly increased (Supplementary Figure 6). Thus, the gene editing of the *Ccnb1* 3′ UTR enabled us to evaluate the PAS1 function using two mouse models: one involving a loss-of-function mutation (PAS1 mutant), and the other involving increased expression of the mRNA with PAS1 3′ UTR on the PAS3 null background. In addition, they allowed us to define the contribution of the mRNA translation with a long 3′ UTR to the cyclin levels during oocyte maturation using the PAS3 loss-of-function mutant.

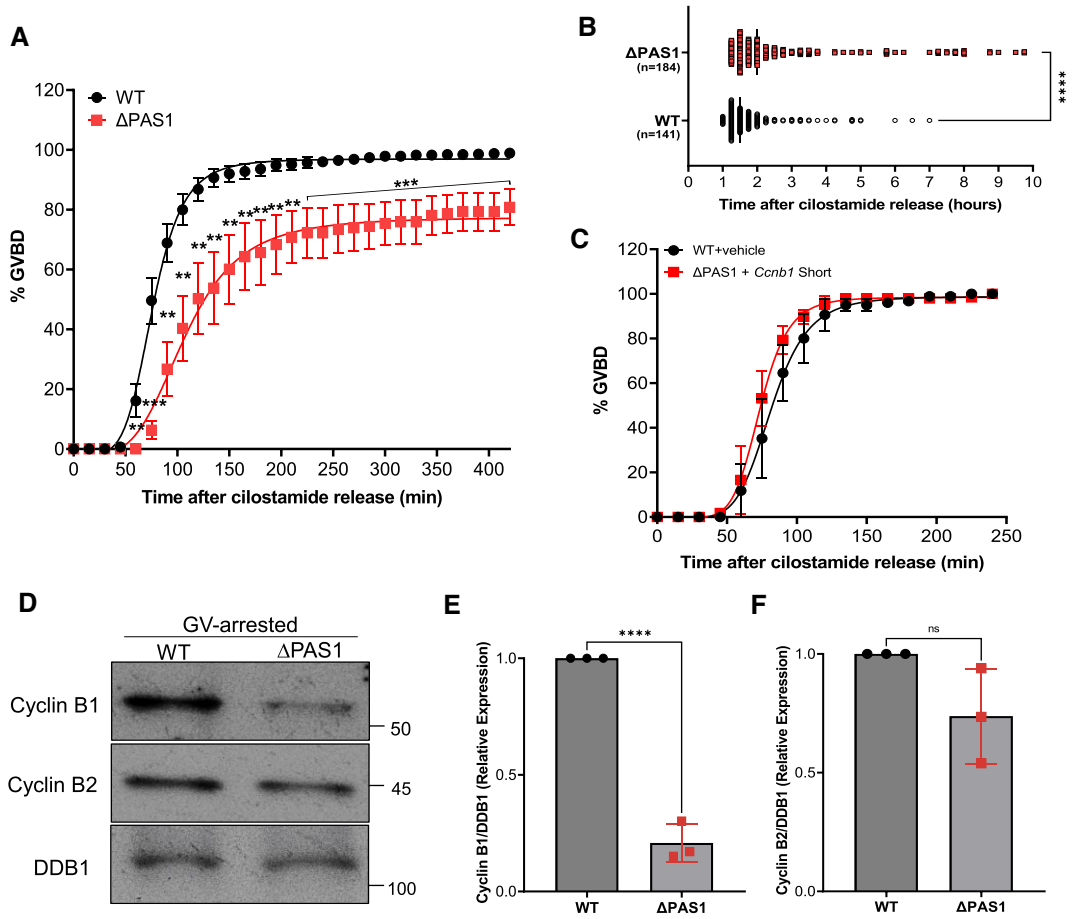

Figure 3. Loss of PAS1 *Ccnb1* variant causes a delay in meiotic resumption. (**A**) Timing of GVBD in cultured denuded oocytes from WT and ΔPAS1 mutant mice. Oocytes were isolated as described in the Methods and timing of GVBD was scored by time-lapse microscopy after release from cilostamide block. Fifteen biological replicates for WT and six for the ΔPAS1 were included. Data were analyzed with non-parametric Mann–Whitney test and the calculated FDR was reported for each time point (* FDR ≤ 0.05; ** FDR ≤ 0.01; *** FDR ≤ 0.001). A four-parameter logistic equation was used to calculate the time when 50% of oocytes had undergone GVBD ($Time_{50\%}$: WT = 76.4 min, 95% confidence limit: 74.1–78.8; ΔPAS1 mutant = 107.4 min, 95% confidence limit: 96.2–120.1) as well as the slope of the curves (Hill coefficient: WT = 5.26, mutant = 3.99). (**B**) Timing of GVBD of individual oocytes from WT and ΔPAS1 mutant determined by time-lapse microscopy. Each point corresponded to one oocyte and the median of all determination was included. Statistical significance was calculated using unpaired *t*-test (**** $P \leq 0.0001$). (**C**) Rescue of the PAS1 GVBD timing in ΔPAS1 oocytes. Denuded oocytes were microinjected with either vehicle (WT) or mRNA where the *Ccnb1* ORF is fused to the intact PAS1 3′UTR (*Ccnb1*-PAS1 injected in ΔPAS1). The time when 50% of oocytes had undergone GVBD ($Time_{50\%}$) was comparable in the two groups (WT = 81.98 min; PAS1 rescue = 73.79). The two curves were not statistically different when using a Mann–Whitney test. (**D**) Representative immunoblots of Cyclin B1 and Cyclin B2 levels in lysates of GV oocytes from WT and ΔPAS1 mutant mice (150 oocytes/lane). DDB1 was used as a loading control. (**E**, **F**) Quantification of (D), relative protein levels of Cyclin B1 and Cyclin B2 in GV oocytes from WT and PAS1 mutant. Three biological replicates were included. Statistical significance was assessed using unpaired *t*-test (**** $P \leq 0.0001$, ns, not significant).

Loss of mRNA generated by PAS1 alternative polyadenylation causes a delay in meiotic resumption

The short and long 3′ UTRs of *Ccnb1* were fused to an enhanced Ypet ORF, transcribed *in vitro*, and then mRNA was microinjected into mouse oocytes arrested in GV (Supplementary Figure 7A). Translation of each transcript was monitored by time-lapse microscopy in quiescent GV oocytes or during oocyte maturation. In agreement with our previous observation using a different reporter system (36), the PAS1 short 3′ UTR drives constitutive translation in GV oocytes, whereas the translation directed by the PAS3 long form is largely repressed in these quiescent oocytes (Supplementary Figure 7B-D). The calculated rates of translation for the short form (0.029 ± 0.002 units/hr) were approximately ten-fold higher than those calculated for the long form (0.0042 ± 0.002 units/hr). Conversely, during oocyte maturation, the translation driven by the long form increased approximately 30-fold whereas a marginal increase (1.5–2-fold) was detected for the short form (Supplementary Figure 7D).

On the basis of the above estimates using an *in vitro* system, we surmised that the inactivation of PAS1 generating the short form should affect either GV oocytes or the early events during meiotic re-entry. Meiotic progression of ΔPAS1 mutant oocytes was monitored by time-lapse microscopy after release from cilostamide, a PDE3 inhibitor that blocks meiotic re-entry. The timing of germinal vesicle breakdown (GVBD) was significantly delayed in PAS1 mutant oocytes compared with WT (Figure 3A,B). Fitting of the maturation curves with a four-parameter logistic equation showed that half of the WT oocytes had undergone GVBD within 76.4 min (95% CI: 74.1–78.8), whereas 107.4 min (95% CI: 96.2–120.1) were

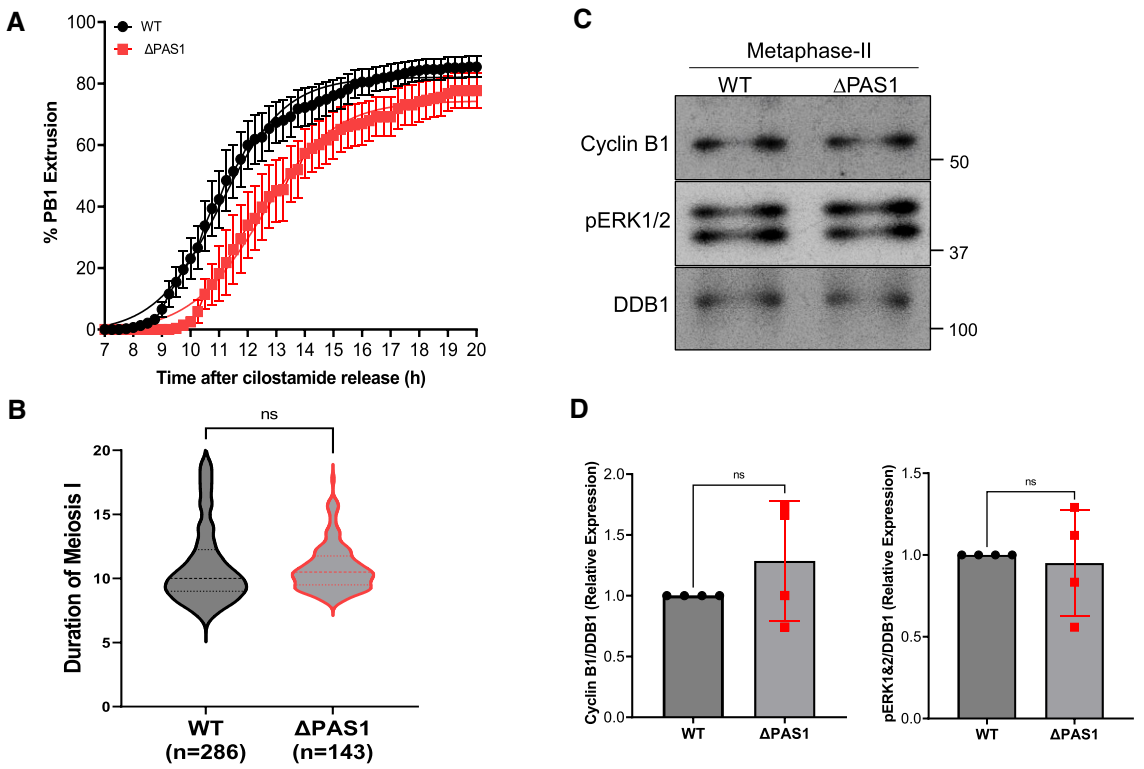

Figure 4. Loss of PAS1 *Ccnb1* variant does not affect mouse oocyte progression to MII. (**A**) Time-lapse microscopy analysis of timing of the first polar body extrusion in WT and PAS1 mutant oocytes after release from cilostamide block. Experiments were repeated 6 times with oocytes retrieved from at least 1 mouse/experiment. The two curves were not statistically different when using a Mann–Whitney test. $Time_{50\%}$: WT = 11.0 min, 95% confidence limit: 10.88–11.20; ΔPAS1 = 12.48 min, 95% confidence limit:12.23–12.75. (**B**) Violin plot of the duration of the first meiotic division in WT and ΔPAS1 oocytes. The duration of the first meiotic division was calculated by subtracting the time of GVBD from the time of PB1 extrusion. Statistical significance was assessed using Mann–Whitney test (ns, not significant). Number of oocytes used for the measurements: WT $n = 286$, ΔPAS1 $n = 143$. (**C**) Representative immunoblot images of Cyclin B1 and pERK1/2 protein levels in metaphase II oocyte lysates from WT and ΔPAS1 mutant (50 oocytes/lane). DDB1 was used as a loading control. (**D**) Quantifications of relative protein expression levels of Cyclin B1 (left) and pERK1/2 (right) in metaphase II oocytes of WT and ΔPAS1 from four biological replicates. Statistical significance was calculated using unpaired *t*-test (ns, not significant).

required for the PAS1 mutant oocytes to reach this stage (Figure 3A). In addition, a different Hill coefficient was also observed (WT: 5.27, 95% CI: 4.6–6.1; ΔPAS1: 3.40, 95% CI: 2.7–6.1), suggesting a decreased cooperative meiotic re-entry.

To verify whether the delay in meiotic re-entry in ΔPAS1 oocytes is indeed the result of the loss of this variant, we conducted a rescue experiment by microinjecting an mRNA with the *Ccnb1* ORF fused to the intact PAS1 3′UTR. This construct was injected into GV-stage ΔPAS1 oocytes, while vehicle-injected WT oocytes were used as a control. Meiotic progression was monitored using time-lapse microscopy following release from the cilostamide block. Under these conditions, the timing of GVBD in ΔPAS1 oocytes was comparable to that of WT, and the two time courses were not significantly different (Figure 3C), providing strong evidence that the phenotypes observed were indeed a direct result of the loss of PAS1 variant.

To investigate whether the phenotype we observed in the ΔPAS1 mutant oocytes is due to insufficient protein levels, we measured Cyclin B1 protein in GV-arrested oocytes by western blot. Inactivation of the proximal PAS1 in *Ccnb1* mRNA 3′ UTR significantly reduced Cyclin B1 protein expression by approximately 70% (Figure 3D,E) compared to WT. No effect on Cyclin B2 levels were observed in the ΔPAS1 mutant mice (Figure 3D, F). Taken together, these data point to an essential role of the short PAS1 3′ UTR in the control of *Ccnb1* mRNA translation in quiescent GV oocytes.

The timing of first polar body extrusion, a readout of the transition to meiosis II (MII), was delayed in oocytes with the ΔPAS1 mutation (Figure 4A); nevertheless, over 70% of them reached MII in a time frame similar to that of WT oocytes (17 h) (Figure 4A). The duration of meiosis I, calculated by subtracting the GVBD time from the time of PB1 extrusion, was not statistically different between WT and ΔPAS1 mutant oocytes (Figure 4B), indicating that after an initial delay, the ΔPAS1 oocytes progressed through the two meiotic divisions with timing comparable to that of WT. This conclusion was further supported by Western blot analysis with MII oocytes, which indicated comparable levels of Cyclin B1 expression in both WT and ΔPAS1 oocytes (Figure 4C, D). Normal levels of ERK1/2 phosphorylation in MII further support the view that phenotypes associated with loss of PAS1 are restricted to the GV/prophase transition (Figure 4C, D), These findings suggest that the decreased Cyclin B1 protein levels in ΔPAS1 mutant are recovered during oocyte maturation to allow normal progression to MII.

Inactivation of PAS3 in *Ccnb1* mRNA 3′ UTR accelerates the re-entry of meiosis in mouse oocytes via MPF activation

As reported above, mutation of PAS3 induced an upregulation of the PAS1 variant (Figure 2B, C). When the time course of meiotic maturation was monitored in these ΔPAS3 mutant

oocytes, a significant accelerated re-entry in the cell cycle was detected, with 90% of the oocytes undergoing GVBD in the first hour of incubation (Figure 5A). Western blot analysis of GV-stage oocytes showed a 3-fold increase in Cyclin B1 protein levels in ΔPAS3 mutant compared with WT (Figure 5B). This premature accumulation of Cyclin B1 is consistent with the view that PAS1 plays a significant role in the regulation of Cyclin B1 accumulation at GV in oocytes.

A rescue experiment to reverse the overexpression of the short PAS1 variant on the ΔPAS3 genetic background could not be performed because targeting the PAS1 variant would likely affect also the PAS3-long form. To instead reproduce the increased levels of the short PAS1 isoform, we injected the *Ccnb1* short construct on a WT background. This overexpression accelerated the timing of GVBD in a manner similar to that observed in the ΔPAS3 oocytes (Figure 5C). Note also that overexpression of *Ccnb1* long construct on a ΔPAS3 background had no effect on the timing of GVBD (Supplementary Figure 8A). This lack of an effect is consistent with the view that the PAS3 variant is largely repressed in GV oocytes.

To confirm that the PAS1 upregulation also results in altered MPF activity at meiotic re-entry, we measured CDK1 activation by incubating WT and PAS3 mutant oocyte extracts with a CDK1 substrate, glutathione-S-transferase-protein phosphatase 1 (GST-PP1), and phosphorylation was quantified with phospho-specific antibodies (pT320-PP1) (48,49). A significant increase in CDK1 activity was observed in ΔPAS3 mutant compared to WT at 1 h after cilostamide release (Figure 5D), suggesting that a premature MPF activation is associated with elevated Cyclin B1 protein levels.

PAS3 mutation in *Ccnb1* mRNA alters the timing of meiotic progression as well as spindle function during maturation

According to our hypothesis, the PAS3 variant becomes highly translated during maturation (36). To explore whether disruption of PAS3 affects additional transitions in meiotic progression, we calculated the duration of meiosis I. When compared to the WT, the duration of meiosis I in ΔPAS3 mutant oocytes was significantly extended (Figure 6A), indicating that the loss of PAS3 function in the *Ccnb1* 3′UTR affects the completion of the first meiotic division. Immunofluorescence analysis following an 8-hour *in vitro* maturation indicated that the progression of each step was delayed in the ΔPAS3 mutant (Supplementary Figure 9). Time-lapse data further demonstrated significantly delayed time of the first polar body extrusion in ΔPAS3 mutant oocytes (Figure 6B), indicating an overall disruption of meiotic progression due to the absence of PAS3-driven translation. After the first polar body extrusion, oocytes re-arrested at metaphase II (MII) until fertilization.

To assess the functionality of the MII spindle, we fixed oocytes after 17 h IVM, and performed immunofluorescence analysis on WT and ΔPAS3 oocytes. Barrel-shaped bipolar MII spindles with chromosomes fully aligned at the metaphase plates were observed in >80% of WT oocytes (Figure 6C, D). Conversely, over 60% of ΔPAS3 mutant oocytes showed spindle defects with one or more chromosomes lagging outside of the metaphase plates (Figure 6C, D). The overexpression of *Ccnb1* long construct on a ΔPAS3 background led to overlapping of WT and mutant curves, indicating a potential rescue of the phenotype (Supplementary Figure 8B). However, the microinjection of the vehicle had an impact on the timing of PBE in WT oocytes as well, rendering the interpretation of the data difficult (Supplementary Figure 8B). Moreover, we observed a trend toward a decrease in Cyclin B1 levels ($P = 0.054$), and significant decreases in CDK1 and pERK1/2 activities in the ΔPAS3 mutant oocytes (Figure 7). These findings support the hypothesis that PAS3-mediated *Ccnb1* translation is necessary to maintain CDK1 and ERK1/2 activity in oocytes arrested at the MII stage. In turn, the decreased CDK1 and pERK1/2 activity likely causes the altered spindle function as reported by others (50). This conclusion is further supported by the finding that the temporal pattern of accumulation of a *Ccnb1*-reporter is altered in ΔPAS3 oocytes compared to WT (Supplementary Figure 10). Positive feedback regulation wherein CDK1 increases the translation of Cyclin B1, which in turn stabilizes CDK1 activity, is likely operating at MII. As a consequence, altered *Ccnb1* accumulation and decreased CDK1 activity result in an altered rate of translation in ΔPAS3 MII oocytes.

Discussion

Cyclin B1 protein abundance is temporally regulated at the transcriptional and post-transcriptional levels during both the mitotic and meiotic cell cycles (20). These oscillations play a key role in the control of the activation of the M phase CDK1 kinase (51). Here, we provide functional evidence that the *Ccnb1* mRNA is expressed in oocytes with multiple 3′ UTRs that direct temporally distinct patterns of translation throughout the meiotic divisions. Our genetic manipulations establish that the *Ccnb1* mRNA variant with a short 3′ UTR plays a key role in setting a threshold accumulation of Cyclin B1 protein in GV-arrested oocytes, thus defining the timing of meiotic re-entry. In this state of quiescence, the *Ccnb1* with the long 3′ UTR does not contribute significantly to cyclin synthesis. Conversely, the translation of the long variant directs Cyclin B1 accumulation at later steps during the MI/MII transition. The short and long variants are generated by the alternative usage of the proximal PAS1 and distal PAS3 elements in the 3′ UTR of this gene. Thus, this 3′UTR-APA plays a key role in cyclin protein synthesis and in setting the timings of initiation and progression through the meiotic cell cycle.

The *Ccnb1* mRNA with short 3′ UTR is expressed at relatively low levels (10–15%) compared to the mRNAs with longer 3′ UTRs (40% and 50% respectively) in mouse oocytes. The mechanisms promoting the preferential accumulation of the distal isoforms in oocytes and somatic cells is not readily apparent. The proximal and distal PAS domains are both canonical PAS elements (1). Inspection of the elements located around the two PAS domains do not provide a clue about the preferential usage of the distal element. An upstream UGUA and a downstream GU-rich elements critical for binding of CFIm/CFIIm (cleavage factor) and CSTF (cleavage stimulatory factor) protein complexes (3,52) are present around both the PAS1 and PAS3 sequences (Supplementary Figure 4C). However, a putative ARE (AU-rich element) is found downstream of the proximal PAS in the long 3′ UTRs. Although this may contribute to decrease the stability of the mRNAs with long 3′ UTRs, it has been also reported that an ELAV protein interacting with an ARE represses usage of proximal PASs (8,53,54). The oocyte expresses a unique Elavl2 protein. Other components of the CPSF are unique to the oocyte includ-

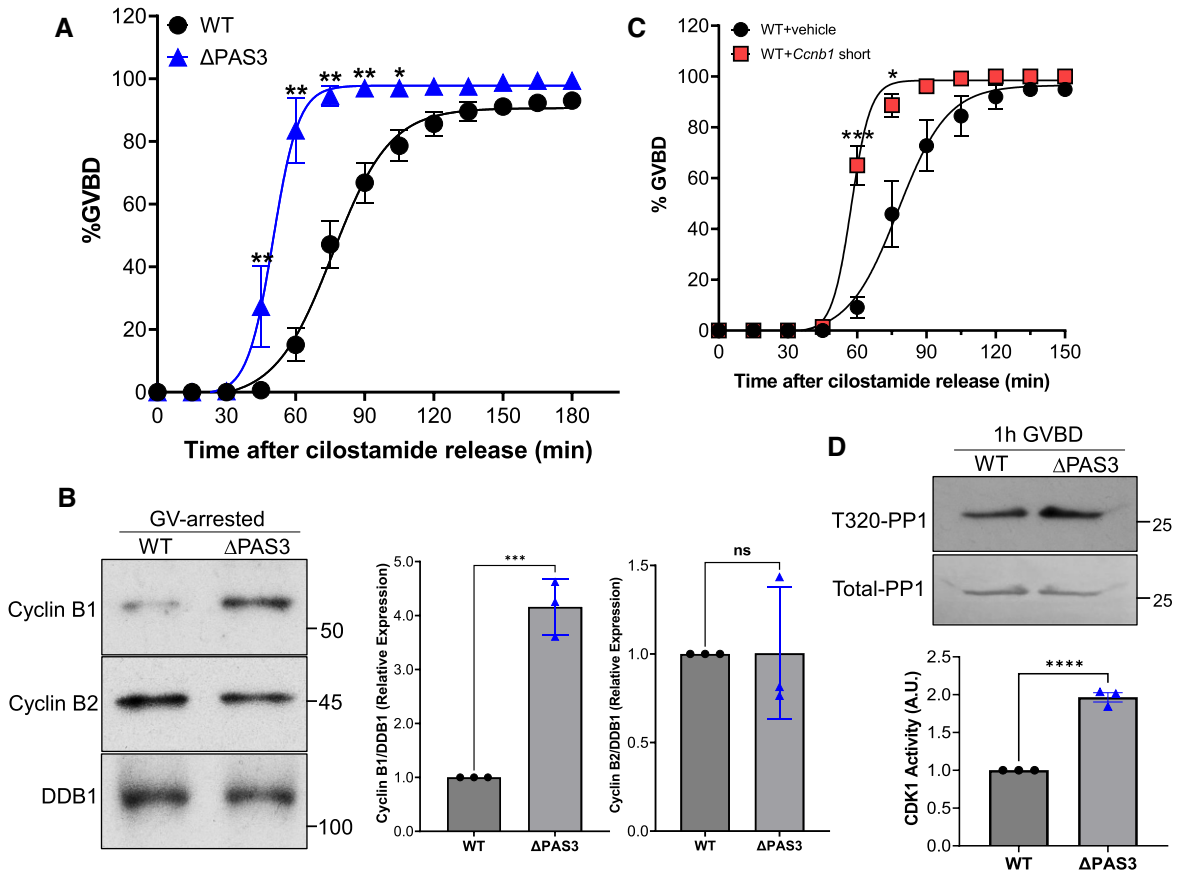

Figure 5. Loss of PAS3 in the *Ccnb1* 3′ UTR leads to premature meiotic re-entry. (**A**) Time-lapse analysis of the timing of GVBD in WT and ΔPAS3 mutant oocytes after release from cilostamide block. Sixteen biological replicates for WT and five for the ΔPAS3 were included. Data were analyzed with non-parametric Mann–Whitney test and the calculated FDR was reported for each time point (*FDR ≤ 0.05; **FDR ≤ 0.01; ***FDR ≤ 0.001). A four-parameter logistic equation was used to calculate the time when 50% of oocytes had undergone GVBD ($Time_{50\%}$: WT = 76.06 min, 95% confidence limit: 72.6–79.6; ΔPAS3 = 50.20 min, 95% confidence limit: 47.92–52.63) as well as the slope of the curves (Hill coefficient: WT = 3.4, mutant = 7.8). (**B**) Representative immunoblot showing expression levels of Cyclin B1 and Cyclin B2 in WT and ΔPAS3 GV-stage oocyte lysates (150 oocytes/lane). DDB1 was used as a loading control. Quantifications of relative protein expression levels of Cyclin B1 (left) and Cyclin B2 (right) in GV-arrested oocytes from WT and ΔPAS3 mice from three biological replicates. Statistical significance was assessed using unpaired t-test (***$P \leq 0.001$, ns, not significant). (**C**) Overexpression of the intact *Ccnb1* PAS1 short variant in WT oocytes causes premature meiotic cell cycle re-entry. WT oocytes were injected with an mRNA coding for PAS1 *Ccnb1* short variant or a vehicle as a control. Timing of GVBD was assessed by time-lapse microscopy. Statistical significance was assessed using Mann–Whitney test (***$P \leq 0.001$, *$P \leq 0.05$). A four-parameter logistic equation was used to calculate the time when 50% of oocytes had undergone GVBD ($Time_{50\%}$: WT + vehicle: 77.68 min, 95% confidence limit: 74.32–81.14; WT + *Ccnb1* short: 57.38 min), as well as the slope of the curves (Hill coefficient: WT + vehicle: 4.0, WT + *Ccnb1* short: 10). (**D**) Representative immunoblot showing the CDK1 activity in WT and ΔPAS3 oocytes 1 h after release from the cilostamide block (20 oocytes/lane). CDK1 activity was measured by phosphorylation level of the CDK1 substrate PP1 as detailed in the Materials and methods. Quantification of CDK1 activity levels between WT and PAS3 mutant from three biological replicates. Statistical significance was assessed using unpaired *t*-test (****$P \leq 0.0001$).

ing a Cpsf4 like (Cpsf4l) subunit of CPSF (37) and a unique homolog of PABN1 (PABN1L or e-PAB) (55). It remains to be determined how the expression of these oocyte specific components of the cleavage and polyadenylation complexes has any impact on the pattern of 3′UTR-APA in the oocyte. The expression of the long and short isoform is interrelated because we show that removal of the PAS in the long 3′ UTR causes an upregulation of the mRNA with short 3′ UTR. This finding is consistent with that observed in somatic cells that the usage of the proximal and the distal PASs are coordinated and that upregulation of one causes the downregulation of the other while overall mRNA levels remain steady (56).

It is less likely that a difference in stability of mRNAs with short and long 3′UTRs underlies the difference in abundance we have observed. Although it has been proposed that mRNAs with long 3′ UTR are less stable than those with short 3′ UTR in somatic cells, in oocytes, it has been reported that mRNAs with short 3′ UTR are less stable than those with long 3′ UTR (57). We have not detected differences in stability when YFP constructs fused to the two 3′ UTRs were expressed both in GV oocytes and during oocyte maturation (36). The different stabilities of mRNAs with short and long 3′ UTRs has been questioned by additional studies (3). It should also be noted that microRNAs, which play a determinant role in destabilizing long but not short isoforms, are not a factor in the oocyte because they are inactive in fully grown oocytes (58).

Although expressed at relatively low abundance, we have predicted that the variant mRNA with short 3′ UTR still would play a role in *Ccnb1* synthesis because it is translated at rates estimated to be up to 10-fold higher than the long forms in quiescent GV oocytes. The phenotypes associated with the PAS1 mutation are consistent with this view.

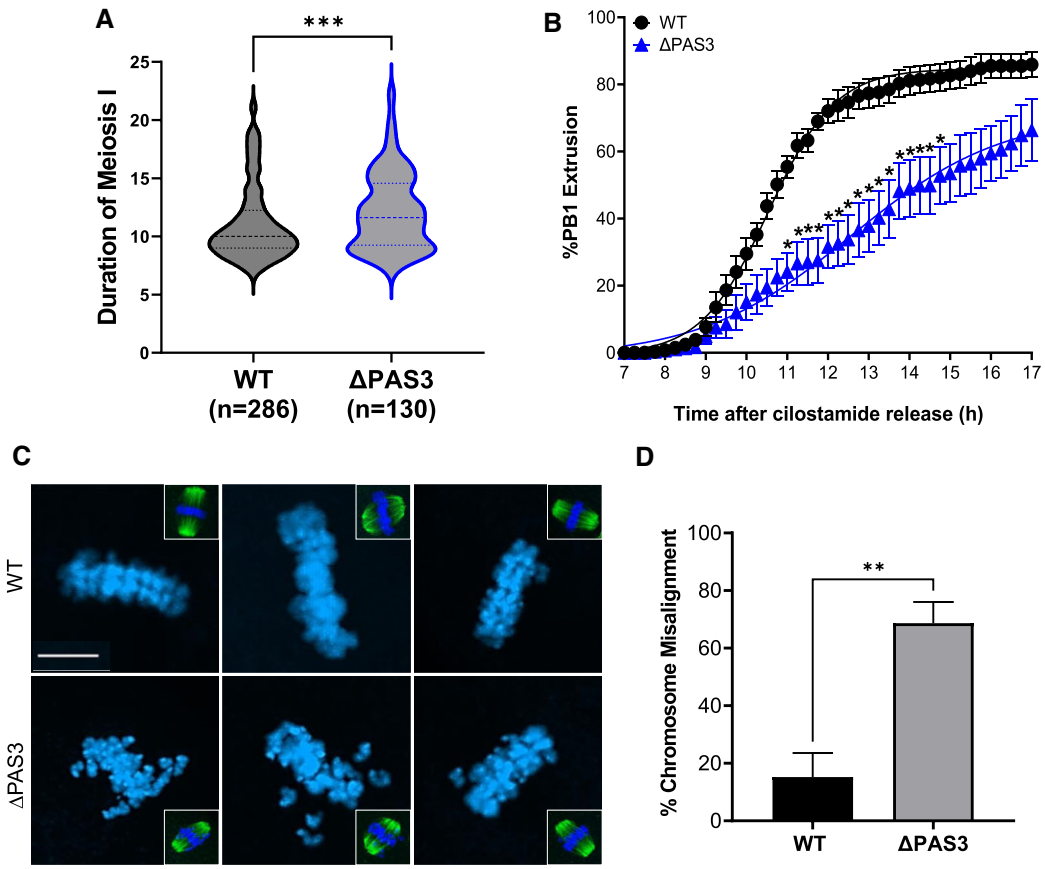

Figure 6. PAS3 *Ccnb1* mRNA long form is required for proper timing of meiotic progression as well as MII spindle function (**A**) Duration of the first meiotic division in WT and ΔPAS3 oocytes. Statistical significance was assessed using Mann–Whitney test (***$P \leq 0.001$). Number of oocytes used for the measurements: WT $n = 286$, ΔPAS3 $n = 130$. (**B**) Time-lapse microscopy analysis for timing of the first polar body extrusion in WT and ΔPAS3 mutant mice after release from cilostamide block. Six biological replicates for WT and five for the ΔPAS3 were included. Data were analyzed with non-parametric Mann–Whitney test and the calculated FDR reported for each time point (* FDR ≤ 0.05). (**C**) Representative confocal images of chromosome congregation at metaphase-II ($n = 3$) in either WT or PAS3 mutant oocytes. DAPI-stained DNA is shown in blue. Scale bar: 10 μm. Insets show whole MII spindles, with microtubules labeled by anti-acetylated α-tubulin antibody (green). (**D**) Quantification of percentage of oocytes with chromosome misalignment. Three biological replicates were analyzed. Statistical significance was assessed using unpaired *t*-test (**$P \leq 0.01$).

Conversely, the translation of the long form is almost undetectable in quiescent GV oocytes because of the presence of CPEs and other regulatory elements that function as repressors of translation in GV oocytes (28,34,59). The presence and functionality of the CPE elements has been documented by several reports including ours (35,36). In addition, the long form may include signals for specific subcellular targeting in GV oocytes when translation is repressed (60). Alternative polyadenylation in neurons is important for local translation of several transcripts at either the dendritic or the axonal localization (61–64).

The two mouse models that we have generated by CRISPR/Cas9 gene editing have enabled us to investigate the role of PAS1 in the generation and translation of the short *Ccnb1* mRNA using both loss-of-function and overexpression. Ablation of PAS1 leads to undetectable short *Ccnb1* mRNA level. This loss-of-function is associated with approximately 70% decrease in Cyclin B1 protein levels in GV oocytes. Because of this decrease, the timing of meiotic re-entry is both delayed and the switch-like properties of this transition are lost (Figure 3A, B). This conclusion is further supported by rescue experiments where microinjection of a *Ccnb1* ORF fused to PAS1 3′ UTR restores the timing of re-entry to WT levels. Conversely, deletion of PAS3 that controls the *Ccnb1* variant with long 3′ UTR is compensated by an increased usage of PAS1 and a 2–3-fold increased abundance of the *Ccnb1* mRNA with the short 3′ UTR. In turn, this increase results in 3–4-fold increase in the steady-state levels of the Cyclin B1 protein in GV oocytes and a premature re-entry into meiotic prophase. Indeed, overexpression of the PAS1 variant mRNA causes an accelerated re-entry into meiosis. The association between premature cell cycle re-entry and elevated PAS1-*Ccnb1* mRNA is also consistent with previous studies showing that increasing Cyclin B1 levels in mouse oocytes induces accelerated timing of GVBD (65–67). A leaky meiotic arrest and premature meiotic re-entry is also associated with the loss of function of f*zr1*, an APC regulator that promotes Cyclin B1 degradation (31).

Recent studies show that the complete inactivation of the *Ccnb1* gene in oocytes causes an upregulation of Cyclin B2, the other cyclin expressed in this quiescent GV stage (68). On the other hand, we report here that the 70% reduction in Cyclin B1 protein associated with PAS1 loss does not trigger an upregulation of Cyclin B2 (Figure 3D,F). A possible explanation to reconcile these differences is that Cyclin B2 compensation is triggered only when more profound changes in Cyclin

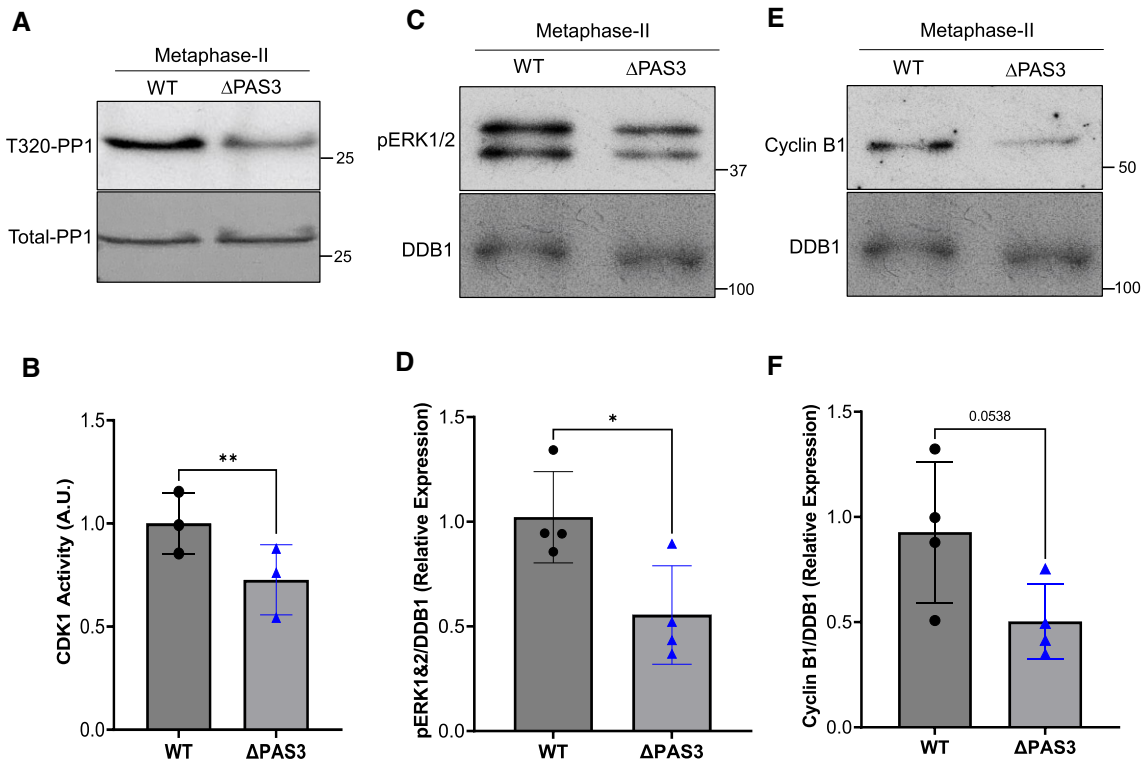

Figure 7. Altered MPF and ERK activities in ΔPAS3 mutant MII-stage oocytes. (**A**) Representative immunoblot showing CDK1 activity in WT and ΔPAS3 MII-stage oocytes (20 oocytes/lane). CDK1 activity was measured by the phosphorylation of the CDK1 substrate PP1 as detailed in the Materials and methods. (**B**) Quantification of CDK1 activity levels between WT and ΔPAS3 mutant from three biological replicates. Statistical significance was assessed using paired *t*-test (** $P \leq 0.01$). (**C**) Representative immunoblot images of pERK1/2 protein levels in metaphase-II oocyte lysates from WT and ΔPAS3 mutant (50 oocytes/lane). DDB1 was used as a loading control. (**D**) Quantifications of pERK1/2 in metaphase-II oocytes in WT and ΔPAS3 oocytes from four biological replicates. Statistical significance was calculated using unpaired *t*-test (* $P \leq 0.05$). (**E**) Representative immunoblot images of Cyclin B1 protein levels in metaphase-II oocyte lysates from WT and ΔPAS3 mutant (50 oocytes/lane). DDB1 was used as a loading control. (**F**) Quantifications of the relative protein levels of Cyclin B1 in metaphase-II oocytes in the WT and ΔPAS3 oocytes from four biological replicates. Statistical significance was reported using paired t-test.

B1 are induced, as in the conditional KO (68). The presence of Cyclin B2 in the ΔPAS1 oocytes is the probable reason why oocytes with a 70% depletion of Cyclin B1 protein still transition from G2 to prophase, albeit with a delayed time course. This finding underscores the overlapping function of Cyclin B1 and Cyclin B2 at meiotic re-entry. The functions of the two cyclins diverge during later stages of meiosis, a finding consistent with the observation that Cyclin B2 does not compensate for the loss of Cyclin B1 in MII (68). In spite of the altered timing of meiotic re-entry, the oocytes lacking the short *Ccnb1* mRNA re-establish normal Cyclin B1 protein levels by MII likely because of the translational activation of the long forms.

In addition to preventing the expression of mRNAs with the short 3′ UTR, our genetic manipulation removes the proximal PAS1 from the long 3′ UTR of *Ccnb1* mRNA. It has been proposed that internal PAS elements in a 3′ UTR have an additional function in the translational control of mRNAs with long 3′ UTRs (69). Our data show that Cyclin B1 protein levels in MII oocytes are comparable to those in control oocytes, suggesting that long forms lacking the proximal PAS element are translated *in vivo* at a rate identical to WT. Moreover, no overt phenotypes other than in the oocytes are observed in homozygous ΔPAS1 mice, suggesting a normal mitotic cell cycle in somatic cells. In contrast to the absence of an effect *in vivo*, we confirmed that PAS1 mutation in the long 3′ UTR decreases the translation of a reporter *in vitro* (Supplementary Figure 11). A possibility is that an unknown compensatory event maintains normal translation *in vivo*, whereas the short-term reporter assay *in vitro* does not allow sufficient time for a compensation. Further experiments are required to reconcile these in *vivo*/*in vitro* differences.

Since oocytes at the GV stage no longer transcribe mRNA, the generation of Cyclin B1 mRNAs of different length mostly occur earlier during oocyte growth when *Ccnb1* mRNA levels in oocytes increase several folds (70). It remains to be determined when the switch from the somatic- to germ cell-specific pattern of *Ccnb1* APA takes place during oocyte development. During fly spermatogenesis, a switch in APA has been observed at the transition from mitosis to meiosis. It is possible that a switch occurs also in oogonia when they enter meiosis in the fetal gonad (71). The differential expression of Cyclin B1 during fly spermatogenesis relies on the presence of transcripts with short and long 3′ UTRs. While the mRNA with the long 3′ UTR predominates in the mitotic spermatogonia, the mRNA with the short 3′ UTR is expressed in meiotic and post-meiotic male germ cells (72). Unlike that found in fly spermatogenesis, Cyclin B1 mRNAs with short and long 3′ UTRs co-exist in mouse oocytes. Consistent with our findings, two species were detected by 3′ RACE in the wildtype fly ovary (73), suggesting that short/long form regulation of

Ccnb1 translation during female meiosis appears early during evolution and is conserved up to mammals (73).

In summary, our findings provide evidence that the pattern of translation of *Ccnb1* mRNA during the specialized meiotic cell cycle is dependent on the differential translation of transcripts with different 3′ UTRs generated by alternative cleavage and polyadenylation. It is likely that similar 3′ UTR-APA-mediated generation of mRNAs with short and long 3′ UTRs defines the pattern of translation of other transcripts during the meiotic cell cycle. Mining of our translation data indeed indicates that, for example, *Wee2*, *CcnO*, *Wapl* and *Pcna* mRNA variants with long and short 3′ UTRs become associated with translating ribosomes at different times during meiosis (36,37). An altered ratio in expression of proximal and distal *Ccnb1* mRNAs also may play a role in the control of replication of oncogenic cells. For instance, overexpression of Cyclin B1 has been observed in numerous tumors (74–76), and its upregulation is strongly associated with a poor prognosis (77,78). Additionally, it is well-established that widespread shortening of 3′ UTRs through cleavage and polyadenylation is a hallmark of oncogenesis (13,14). Within the 3′ UTR of the human *Ccnb1* gene, multiple PAS elements are present, with two located in close proximity to the PAS1 element we have characterized in the mouse *Ccnb1* mRNA. According to the PolyASite 2.0 APA atlas (https://polyasite.unibas.ch/) (Supplementary Table 3), these proximal PAS elements are extensively utilized in human mRNAs. However, it is important to note that this Atlas primarily relies on data from transformed cells. Therefore, one can hypothesize that the elevated levels of *Ccnb1* observed in transformed cells are driven, akin to mouse oocytes, by the preferential utilization of these proximal PAS elements. Further experiments are necessary to validate this possibility.

Data availability

The data included in this article are available in the article and in its online supplementary material. All data are available from the authors upon reasonable request.

Supplementary data

Supplementary Data are available at NAR Online.

Acknowledgements

The authors are thankful to Drs Nozomi Takahashi and Chisato Kunitomi for the helpful discussions and guidance in conducting some of the experiments.

Funding

NIH [R01 GM116926]; NIH/NICHD [P50 HD055764]; Center for Research and Innovation and Training in Reproduction and Infertility (to M.C.); X.W. is supported by a Lalor Foundation fellowship; J.O.B. and F.S.L. were supported by NIH/NIDCR [R35DE031926]. Funding for open access charge: National Institute of General Medicine Sciences.

Conflict of interest statement

None declared.

References

1. Tian,B. and Manley,J.L. (2017) Alternative polyadenylation of mRNA precursors. *MNat. Rev. Mol. Cell Biol.*, **18**, 18–30.
2. Di Giammartino,D.C., Nishida,K. and Manley,J.L. (2011) Mechanisms and consequences of alternative polyadenylation. *Mol. Cell*, **43**, 853–866.
3. Mitschka,S. and Mayr,C. (2022) Context-specific regulation and function of mRNA alternative polyadenylation. *Nat. Rev. Mol. Cell Biol.*, **23**, 779–796.
4. Gruber,A.J. and Zavolan,M. (2019) Alternative cleavage and polyadenylation in health and disease. *Nat. Rev. Genet.*, **20**, 599–614.
5. Ji,Z. and Tian,B. (2009) Reprogramming of 3' untranslated regions of mRNAs by alternative polyadenylation in generation of pluripotent stem cells from different cell types. *PLoS One*, **4**, e8419.
6. Bartel,D.P. (2009) MicroRNAs: target recognition and regulatory functions. *Cell*, **136**, 215–233.
7. Lee,Y.S. and Dutta,A. (2007) The tumor suppressor microRNA let-7 represses the HMGA2 oncogene. *Genes Dev.*, **21**, 1025–1030.
8. Hilgers,V., Perry,M.W., Hendrix,D., Stark,A., Levine,M. and Haley,B. (2011) Neural-specific elongation of 3' UTRs during Drosophila development. *Proc. Natl. Acad. Sci. U.S.A.*, **108**, 15864–15869.
9. Derti,A., Garrett-Engele,P., Macisaac,K.D., Stevens,R.C., Sriram,S., Chen,R., Rohl,C.A., Johnson,J.M. and Babak,T. (2012) A quantitative atlas of polyadenylation in five mammals. *Genome Res.*, **22**, 1173–1183.
10. Smibert,P., Miura,P., Westholm,J.O., Shenker,S., May,G., Duff,M.O., Zhang,D., Eads,B.D., Carlson,J., Brown,J.B., *et al.* (2012) Global patterns of tissue-specific alternative polyadenylation in Drosophila. *Cell Rep.*, **1**, 277–289.
11. Bae,B. and Miura,P. (2020) Emerging roles for 3' UTRs in neurons. *Int. J. Mol. Sci.*, **21**, 3413.
12. Sandberg,R., Neilson,J.R., Sarma,A., Sharp,P.A. and Burge,C.B. (2008) Proliferating cells express mRNAs with shortened 3' untranslated regions and fewer microRNA target sites. *Science*, **320**, 1643–1647.
13. Mayr,C. and Bartel,D.P. (2009) Widespread shortening of 3'UTRs by alternative cleavage and polyadenylation activates oncogenes in cancer cells. *Cell*, **138**, 673–684.
14. Fu,Y., Sun,Y., Li,Y., Li,J., Rao,X., Chen,C. and Xu,A. (2011) Differential genome-wide profiling of tandem 3' UTRs among human breast cancer and normal cells by high-throughput sequencing. *Genome Res.*, **21**, 741–747.
15. Eppig,J.J., O'Brien,M. and Wigglesworth,K. (1996) Mammalian oocyte growth and development in vitro. *Mol. Reprod. Dev.*, **44**, 260–273.
16. Li,R. and Albertini,D.F. (2013) The road to maturation: somatic cell interaction and self-organization of the mammalian oocyte. *Nat. Rev. Mol. Cell Biol.*, **14**, 141–152.
17. Schultz,R.M. (2005) From egg to embryo: a peripatetic journey. *Reproduction*, **130**, 825–828.
18. Conti,M. and Franciosi,F. (2018) Acquisition of oocyte competence to develop as an embryo: integrated nuclear and cytoplasmic events. *Hum. Reprod. Update*, **24**, 245–266.
19. Jones,K.T. (2004) Turning it on and off: m-phase promoting factor during meiotic maturation and fertilization. *Mol. Hum. Reprod.*, **10**, 1–5.
20. Kishimoto,T. (2018) MPF-based meiotic cell cycle control: half a century of lessons from starfish oocytes. *Proc. Jpn. Acad. Ser. B. Phys. Biol. Sci.*, **94**, 180–203.
21. Masui,Y. (2001) From oocyte maturation to the in vitro cell cycle: the history of discoveries of Maturation-Promoting Factor (MPF) and Cytostatic Factor (CSF). *Differentiation*, **69**, 1–17.
22. Li,J., Qian,W.P. and Sun,Q.Y. (2019) Cyclins regulating oocyte meiotic cell cycle progressiondagger. *Biol. Reprod.*, **101**, 878–881.
23. Bouftas,N. and Wassmann,K. (2019) Cycling through mammalian meiosis: b-type cyclins in oocytes. *Cell Cycle*, **18**, 1537–1548.

24. Brandeis,M., Rosewell,I., Carrington,M., Crompton,T., Jacobs,M.A., Kirk,J., Gannon,J. and Hunt,T. (1998) Cyclin B2-null mice develop normally and are fertile whereas cyclin B1-null mice die in utero. *Proc. Natl. Acad. Sci. U.S.A.*, **95**, 4344–4349.
25. Karasu,M.E., Bouftas,N., Keeney,S. and Wassmann,K. (2019) Cyclin B3 promotes anaphase I onset in oocyte meiosis. *J. Cell Biol.*, **218**, 1265–1281.
26. Bouftas,N., Schneider,L., Halder,M., Demmig,R., Baack,M., Cladiere,D., Walter,M., Al Abdallah,H., Kleinhempel,C., Messaritaki,R., *et al.* (2022) Cyclin B3 implements timely vertebrate oocyte arrest for fertilization. *Dev. Cell*, **57**, 2305–2320.
27. Li,Y., Wang,L., Zhang,L., He,Z., Feng,G., Sun,H., Wang,J., Li,Z., Liu,C., Han,J., *et al.* (2019) Cyclin B3 is required for metaphase to anaphase transition in oocyte meiosis I. *J. Cell Biol.*, **218**, 1553–1563.
28. Han,S.J., Martins,J.P.S., Yang,Y., Kang,M.K., Daldello,E.M. and Conti,M. (2017) The translation of cyclin B1 and B2 is differentially regulated during mouse oocyte reentry into the meiotic cell cycle. *Sci. Rep.*, **7**, 14077.
29. Daldello,E.M., Luong,X.G., Yang,C.R., Kuhn,J. and Conti,M. (2019) Cyclin B2 is required for progression through meiosis in mouse oocytes. *Development*, **146**, dev172734.
30. Reis,A., Chang,H.Y., Levasseur,M. and Jones,K.T. (2006) APCcdh1 activity in mouse oocytes prevents entry into the first meiotic division. *Nat. Cell Biol.*, **8**, 539–540.
31. Holt,J.E., Tran,S.M., Stewart,J.L., Minahan,K., Garcia-Higuera,I., Moreno,S. and Jones,K.T. (2011) The APC/C activator FZR1 coordinates the timing of meiotic resumption during prophase I arrest in mammalian oocytes. *Development*, **138**, 905–913.
32. Marangos,P., Verschuren,E.W., Chen,R., Jackson,P.K. and Carroll,J. (2007) Prophase I arrest and progression to metaphase I in mouse oocytes are controlled by Emi1-dependent regulation of APC(Cdh1). *J. Cell Biol.*, **176**, 65–75.
33. Conti,M. and Kunitomi,C. (2023) A genome-wide perspective of the maternal mRNA translation program during oocyte development. *Semin. Cell Dev. Biol.*, **154**, 88–98.
34. Richter,J.D. (2007) CPEB: a life in translation. *Trends Biochem. Sci.*, **32**, 279–285.
35. Tay,J., Hodgman,R. and Richter,J.D. (2000) The control of cyclin B1 mRNA translation during mouse oocyte maturation. *Dev. Biol.*, **221**, 1–9.
36. Yang,Y., Yang,C.R., Han,S.J., Daldello,E.M., Cho,A., Martins,J.P.S., Xia,G. and Conti,M. (2017) Maternal mRNAs with distinct 3' UTRs define the temporal pattern of Ccnb1 synthesis during mouse oocyte meiotic maturation. *Genes Dev.*, **31**, 1302–1307.
37. Luong,X.G., Daldello,E.M., Rajkovic,G., Yang,C.R. and Conti,M. (2020) Genome-wide analysis reveals a switch in the translational program upon oocyte meiotic resumption. *Nucleic Acids Res.*, **48**, 3257–3276.
38. Pique,M., Lopez,J.M., Foissac,S., Guigo,R. and Mendez,R. (2008) A combinatorial code for CPE-mediated translational control. *Cell*, **132**, 434–448.
39. Tay,J., Hodgman,R., Sarkissian,M. and Richter,J.D. (2003) Regulated CPEB phosphorylation during meiotic progression suggests a mechanism for temporal control of maternal mRNA translation. *Genes Dev.*, **17**, 1457–1462.
40. Mendez,R., Murthy,K.G., Ryan,K., Manley,J.L. and Richter,J.D. (2000) Phosphorylation of CPEB by Eg2 mediates the recruitment of CPSF into an active cytoplasmic polyadenylation complex. *Mol. Cell*, **6**, 1253–1259.
41. Minshall,N., Reiter,M.H., Weil,D. and Standart,N. (2007) CPEB interacts with an ovary-specific eIF4E and 4E-T in early Xenopus oocytes. *J. Biol. Chem.*, **282**, 37389–37401.
42. Duran-Arque,B., Canete,M., Castellazzi,C.L., Bartomeu,A., Ferrer-Caelles,A., Reina,O., Caballe,A., Gay,M., Arauz-Garofalo,G., Belloc,E., *et al.* (2022) Comparative analyses of vertebrate CPEB proteins define two subfamilies with coordinated yet distinct functions in post-transcriptional gene regulation. *Genome Biol.*, **23**, 192.
43. Gurumurthy,C.B., Sato,M., Nakamura,A., Inui,M., Kawano,N., Islam,M.A., Ogiwara,S., Takabayashi,S., Matsuyama,M., Nakagawa,S., *et al.* (2019) Creation of CRISPR-based germline-genome-engineered mice without ex vivo handling of zygotes by i-GONAD. *Nat. Protoc.*, **14**, 2452–2482.
44. Ohtsuka,M., Sato,M., Miura,H., Takabayashi,S., Matsuyama,M., Koyano,T., Arifin,N., Nakamura,S., Wada,K. and Gurumurthy,C.B. (2018) i-GONAD: a robust method for in situ germline genome engineering using CRISPR nucleases. *Genome Biol.*, **19**, 25.
45. Liu,Y., Nie,H., Liu,H. and Lu,F. (2019) Poly(A) inclusive RNA isoform sequencing (PAIso-seq) reveals wide-spread non-adenosine residues within RNA poly(A) tails. *Nat. Commun.*, **10**, 5292.
46. Yusheng Liu,H.N., Wang,L.-Y., Wu,S., Li,W., Zhou,Q., Wang,J. and Lu,F. (2021) Abundant non-A residues in the poly(A) tail orchestrate the mouse oocyte-to-embryo transition. bioRxiv doi: https://doi.org/10.1101/2021.08.29.458077, 31 August 2021,preprint: not peer reviewed.
47. Herrmann,C.J., Schmidt,R., Kanitz,A., Artimo,P., Gruber,A.J. and Zavolan,M. (2020) PolyASite 2.0: a consolidated atlas of polyadenylation sites from 3' end sequencing. *Nucleic Acids Res.*, **48**, D174–D179.
48. Daldello,E.M., Le,T., Poulhe,R., Jessus,C., Haccard,O. and Dupre,A. (2015) Control of Cdc6 accumulation by Cdk1 and MAPK is essential for completion of oocyte meiotic divisions in Xenopus. *J. Cell Sci.*, **128**, 2482–2496.
49. Lewis,C.W., Taylor,R.G., Kubara,P.M., Marshall,K., Meijer,L. and Golsteyn,R.M. (2013) A western blot assay to measure cyclin dependent kinase activity in cells or in vitro without the use of radioisotopes. *FEBS Lett.*, **587**, 3089–3095.
50. Zhang,Y.L., Liu,X.M., Ji,S.Y., Sha,Q.Q., Zhang,J. and Fan,H.Y. (2015) ERK1/2 activities are dispensable for oocyte growth but are required for meiotic maturation and pronuclear formation in mouse. *J. Genet Genomics*, **42**, 477–485.
51. Ferrell,J.E. Jr (1999) Building a cellular switch: more lessons from a good egg. *Bioessays*, **21**, 866–870.
52. Hu,J., Lutz,C.S., Wilusz,J. and Tian,B. (2005) Bioinformatic identification of candidate cis-regulatory elements involved in human mRNA polyadenylation. *RNA*, **11**, 1485–1493.
53. Oktaba,K., Zhang,W., Lotz,T.S., Jun,D.J., Lemke,S.B., Ng,S.P., Esposito,E., Levine,M. and Hilgers,V. (2015) ELAV links paused Pol II to alternative polyadenylation in the Drosophila nervous system. *Mol. Cell*, **57**, 341–348.
54. Hilgers,V., Lemke,S.B. and Levine,M. (2012) ELAV mediates 3' UTR extension in the Drosophila nervous system. *Genes Dev.*, **26**, 2259–2264.
55. Guzeloglu-Kayisli,O., Lalioti,M.D., Aydiner,F., Sasson,I., Ilbay,O., Sakkas,D., Lowther,K.M., Mehlmann,L.M. and Seli,E. (2012) Embryonic poly(A)-binding protein (EPAB) is required for oocyte maturation and female fertility in mice. *Biochem. J.*, **446**, 47–58.
56. Spies,N., Burge,C.B. and Bartel,D.P. (2013) 3' UTR-isoform choice has limited influence on the stability and translational efficiency of most mRNAs in mouse fibroblasts. *Genome Res.*, **23**, 2078–2090.
57. Freimer,J.W., Krishnakumar,R., Cook,M.S. and Blelloch,R. (2018) Expression of alternative Ago2 isoform associated with loss of microRNA-driven translational repression in mouse oocytes. *Curr. Biol.*, **28**, 296–302.
58. Suh,N., Baehner,L., Moltzahn,F., Melton,C., Shenoy,A., Chen,J. and Blelloch,R. (2010) MicroRNA function is globally suppressed in mouse oocytes and early embryos. *Curr. Biol.*, **20**, 271–277.
59. Richter,J.D. and Lasko,P. (2011) Translational control in oocyte development. *Cold Spring Harb. Perspect. Biol.*, **3**, a002758.
60. Kotani,T., Yasuda,K., Ota,R. and Yamashita,M. (2013) Cyclin B1 mRNA translation is temporally controlled through formation and disassembly of RNA granules. *J. Cell Biol.*, **202**, 1041–1055.
61. Shigeoka,T., Jung,H., Jung,J., Turner-Bridger,B., Ohk,J., Lin,J.Q., Amieux,P.S. and Holt,C.E. (2016) Dynamic axonal translation in developing and mature visual circuits. *Cell*, **166**, 181–192.
62. Taliaferro,J.M., Vidaki,M., Oliveira,R., Olson,S., Zhan,L., Saxena,T., Wang,E.T., Graveley,B.R., Gertler,F.B., Swanson,M.S.,

et al. (2016) Distal alternative last exons localize mRNAs to neural projections. *Mol. Cell*, **61**, 821–833.
63. Tushev,G., Glock,C., Heumuller,M., Biever,A., Jovanovic,M. and Schuman,E.M. (2018) Alternative 3' UTRs modify the localization, regulatory potential, stability, and plasticity of mRNAs in neuronal compartments. *Neuron*, **98**, 495–511.
64. Andreassi,C., Luisier,R., Crerar,H., Darsinou,M., Blokzijl-Franke,S., Lenn,T., Luscombe,N.M., Cuda,G., Gaspari,M., Saiardi,A., *et al.* (2021) Cytoplasmic cleavage of IMPA1 3' UTR is necessary for maintaining axon integrity. *Cell Rep.*, **34**, 108778.
65. Ledan,E., Polanski,Z., Terret,M.E. and Maro,B. (2001) Meiotic maturation of the mouse oocyte requires an equilibrium between cyclin B synthesis and degradation. *Dev. Biol.*, **232**, 400–413.
66. Marangos,P. and Carroll,J. (2004) The dynamics of cyclin B1 distribution during meiosis I in mouse oocytes. *Reproduction*, **128**, 153–162.
67. Holt,J.E., Weaver,J. and Jones,K.T. (2010) Spatial regulation of APCCdh1-induced cyclin B1 degradation maintains G2 arrest in mouse oocytes. *Development*, **137**, 1297–1304.
68. Li,J., Tang,J.X., Cheng,J.M., Hu,B., Wang,Y.Q., Aalia,B., Li,X.Y., Jin,C., Wang,X.X., Deng,S.L., *et al.* (2018) Cyclin B2 can compensate for Cyclin B1 in oocyte meiosis I. *J. Cell Biol.*, **217**, 3901–3911.
69. Dai,X.X., Jiang,J.C., Sha,Q.Q., Jiang,Y., Ou,X.H. and Fan,H.Y. (2019) A combinatorial code for mRNA 3'-UTR-mediated translational control in the mouse oocyte. *Nucleic Acids Res.*, **47**, 328–340.
70. Pan,H., O'Brien M,J., Wigglesworth,K., Eppig,J.J. and Schultz,R.M. (2005) Transcript profiling during mouse oocyte development and the effect of gonadotropin priming and development in vitro. *Dev. Biol.*, **286**, 493–506.
71. Seydoux,G. and Braun,R.E. (2006) Pathway to totipotency: lessons from germ cells. *Cell*, **127**, 891–904.
72. Berry,C.W., Olivares,G.H., Gallicchio,L., Ramaswami,G., Glavic,A., Olguin,P., Li,J.B. and Fuller,M.T. (2022) Developmentally regulated alternate 3' end cleavage of nascent transcripts controls dynamic changes in protein expression in an adult stem cell lineage. *Genes Dev.*, **36**, 916–935.
73. Baker,C.C., Gim,B.S. and Fuller,M.T. (2015) Cell type-specific translational repression of Cyclin B during meiosis in males. *Development*, **142**, 3394–3402.
74. Yin,X.Y., Grove,L., Datta,N.S., Katula,K., Long,M.W. and Prochownik,E.V. (2001) Inverse regulation of cyclin B1 by c-Myc and p53 and induction of tetraploidy by cyclin B1 overexpression. *Cancer Res.*, **61**, 6487–6493.
75. Soria,J.C., Jang,S.J., Khuri,F.R., Hassan,K., Liu,D., Hong,W.K. and Mao,L. (2000) Overexpression of cyclin B1 in early-stage non-small cell lung cancer and its clinical implication. *Cancer Res.*, **60**, 4000–4004.
76. Agarwal,R., Gonzalez-Angulo,A.M., Myhre,S., Carey,M., Lee,J.S., Overgaard,J., Alsner,J., Stemke-Hale,K., Lluch,A., Neve,R.M., *et al.* (2009) Integrative analysis of cyclin protein levels identifies cyclin b1 as a classifier and predictor of outcomes in breast cancer. *Clin. Cancer Res.*, **15**, 3654–3662.
77. Murakami,H., Furihata,M., Ohtsuki,Y. and Ogoshi,S. (1999) Determination of the prognostic significance of cyclin B1 overexpression in patients with esophageal squamous cell carcinoma. *Virchows. Arch.*, **434**, 153–158.
78. Wang,A., Yoshimi,N., Ino,N., Tanaka,T. and Mori,H. (1997) Overexpression of cyclin B1 in human colorectal cancers. *J. Cancer Res. Clin. Oncol.*, **123**, 124–127.

Received: June 16, 2023. **Revised:** November 1, 2023. **Editorial Decision:** November 13, 2023. **Accepted:** November 14, 2023